Cell PRESS
Neuron
Report

Development of Cell Type-Specific Connectivity Patterns of Converging Excitatory Axons in the Retina

Joshua L. Morgan,[1,3] Florentina Soto,[2] Rachel O.L. Wong,[1] and Daniel Kerschensteiner[1,2,*]
[1]Department of Biological Structure, University of Washington School of Medicine, 1959 NE Pacific Street, Seattle, WA 98195, USA
[2]Department of Ophthalmology and Visual Sciences, Washington University School of Medicine, 660 S. Euclid Avenue, Saint Louis, MO 63110, USA
[3]Present address: Department of Neurobiology, Harvard Medical School, 220 Longwood Avenue, Boston, MA 02115, USA
*Correspondence: dkerschensteiner@wustl.edu
DOI 10.1016/j.neuron.2011.08.025

SUMMARY

To integrate information from different presynaptic cell types, dendrites receive distinct patterns of synapses from converging axons. How different afferents in vivo establish specific connectivity patterns with the same dendrite is poorly understood. Here, we examine the synaptic development of three glutamatergic bipolar cell types converging onto a common postsynaptic retinal ganglion cell. We find that after axons and dendrites target appropriate synaptic layers, patterns of connections among these neurons diverge through selective changes in the conversion of axo-dendritic appositions to synapses. This process is differentially regulated by neurotransmission, which is required for the shift from single to multisynaptic appositions of one bipolar cell type but not for maintenance and elimination, respectively, of connections from the other two types. Thus, synaptic specificity among converging excitatory inputs in the retina emerges via differential synaptic maturation of axo-dendritic appositions and is shaped by neurotransmission in a cell type-dependent manner.

INTRODUCTION

The flow of information through neural circuits depends on the patterns of synapses that connect their constituent cells. In particular, the ability of presynaptic neurons to elicit action potentials from postsynaptic targets depends on the number and distribution of synapses connecting the respective axons and dendrites (Silver, 2010; Spruston, 2008). We know little about the cellular mechanisms and signals that enable developing axons in vivo to establish specific patterns of synapses, especially when different presynaptic cell types converge onto a shared postsynaptic target.

The development of axonal connections has mostly been studied in circuits like the neuromuscular junction (NMJ), where the target initially is innervated by multiple afferents of which all but one are later eliminated (Brown et al., 1976). At the NMJ, the winning axon expands as it takes over synaptic territory vacated by retracting axons (Walsh and Lichtman, 2003). Similarly, the single climbing fiber that remains connected to a given Purkinje cell grows and ascends along the proximal dendrite while others withdraw (Hashimoto et al., 2009). These studies have established a link between axonal growth and retraction, and synapse formation and elimination, respectively, in circuits where the remaining axon is the sole occupant of the postsynaptic territory it innervates.

However, whether changes in axon morphology similarly shape the development of circuits in which dendrites maintain synapses from multiple afferents is unclear. Indeed, many neurons in the central nervous system receive excitatory input from different presynaptic cell types that communicate distinct information via axons that overlap and synapses that intermingle on the target dendrite (Shepherd, 2004). The cellular mechanisms that establish cell type-specific patterns of connections from convergent axons sharing dendritic space remain unknown in part because the cellular identity of long-range afferent projections involved in many CNS circuits is difficult to trace. Here, we took advantage of the short range and laminar organization of bipolar cell (BC) projections in the vertebrate retina to determine how converging excitatory inputs attain cell type-specific connectivity.

In addition to the cellular rearrangements that establish synaptic specificity among converging excitatory inputs, the signals which instruct these rearrangements are poorly understood. We previously found that glutamate release from BCs regulates the total number of synapses formed on retinal ganglion cell (RGC) dendrites (Kerschensteiner et al., 2009). Here, we test whether this regulation depends on the afferent cell type and thus shapes the development of specific connectivity patterns.

Twelve types of BCs relay different components of photoreceptor signals from the outer to the inner plexiform layer (IPL) of the retina (Wässle et al., 2009). As in many other parts of the nervous system, connections in the IPL are organized into laminar circuits (Sanes and Zipursky, 2010; Wässle, 2004). Accordingly, axons of different BC types target distinct depths of the IPL where they innervate RGCs that stratify their dendrites at the same depth. Developing BCs elaborate axonal arbors from neuroepithelial-like precursor processes, extending side branches throughout the IPL of which they selectively stabilize those located at the correct depth (Morgan et al., 2006). BC

axons attain their final laminar position before the retina processes visual information and continue to form and eliminate synapses with RGC dendrites at high rates for more than a week after laminar targeting is complete (Kerschensteiner et al., 2009; Morgan et al., 2008). How retinal circuits are rewired by this synaptic remodeling after laminar targeting remains unknown.

Combining different genetic labeling techniques and imaging approaches we examined the development of synapses from three types of BCs with a single type of RGC in vivo. We find that the different BC axons initially connect equally to the shared RGC dendrite. Synaptic patterns of the different BC types diverge only after laminar targeting is complete. This is achieved by selective changes in the conversion of axo-dendritic appositions to synapses. Neurotransmission regulates this process in a cell type-dependent manner and thus shapes synaptic specificity among converging excitatory axons.

RESULTS

Cell Type-Specific Development of Axonal Connectivity

To observe directly how different afferents establish specific patterns of connections with a common target, we fluorescently labeled pairs of neurons and their connections in the intact developing retina. Pairs consisted of one of three BC types and a single RGC type.

Of the twelve BC types found in mice (Wässle et al., 2009) eleven receive input from cone photoreceptors and one from rods. Five cone BC types (B1, B2, B3a, B3b, B4) express ionotropic glutamate receptors on their dendrites and depolarize in response to light decrements (OFF BCs) (Haverkamp et al., 2001a, 2001b). The single rod BC type (RB) and six cone BC types (B5a, B5b, B6–9) employ a metabotropic glutamate receptor (protein, mGluR6; gene, *Grm6*) to invert the photoreceptor signal and depolarize to light increments (ON BCs) (Nomura et al., 1994; Vardi et al., 2000). The individual ON and OFF BC types further communicate distinct temporal, spatial, and spectral components of visual information (Breuninger et al., 2011; Freed, 2000; Li and DeVries, 2006). We previously generated transgenic mice in which a fragment of the *Grm6* promoter drives expression of the red fluorescent protein tandem dimer Tomato (*Grm6-tdTomato*), from early postnatal development (postnatal day 5, P5) on (Kerschensteiner et al., 2009). We took advantage of random integration effects and selected a founder line in which only a small percentage of ON BCs fluoresce brightly (see Figures S1A and S1B available online). In this line, we could reliably reconstruct axons of single BCs and assign cell types based on their characteristic stratification depths and branching patterns. Most ON BCs identified in this way belonged to B6, B7, or RB types (Ghosh et al., 2004; Wässle et al., 2009). We further used antibodies against PKCα and synaptotagmin2 to label B6 and RB cells, respectively (Figures S1A and S1B; Fox and Sanes, 2007; Masu et al., 1995). This confirmed, in all cases, the morphology-based classification of the BCs types we examined.

To simultaneously label RGC dendrites and glutamatergic synapses from BCs, we biolistically transfected dispersed RGCs in *Grm6-tdTomato* retinas with cerulean fluorescent protein (CFP) and postsynaptic density protein 95 fused to yellow fluorescent protein (PSD95-YFP) (Morgan and Kerschensteiner, 2011). We previously showed that PSD95-YFP in RGCs localizes selectively to BC synapses and does not interfere with synaptogenesis (Kerschensteiner et al., 2009; Morgan et al., 2008). Biolistics can label all ~20 morphological RGCs types. Because mostly B6, B7, and RB cells are labeled in *Grm6-tdTomato* mice, we restricted our analysis to G10 RGCs, which are targeted by the axons of these BC types (Völgyi et al., 2009). In addition, the highly characteristic dendritic morphology of G10 RGCs allowed us to reliably identify these cells from postnatal day 9 (P9) onward (Figures S1C and S1D). The combination of transgenic and biolistic labeling enabled us to directly examine the connectivity of pairs of specific neuronal cell types in intact developing retinal circuits (Figures 1A and 1B).

To compare the synaptic development of converging axons, we counted the connections among B6, B7, and RB axons and G10 dendrites at P9 and P21. By P9, both axons and dendrites have stratified and assumed cell type-specific morphologies (Coombs et al., 2007; Diao et al., 2004; Morgan et al., 2006; Stacy and Wong, 2003). However, synapses continue to be formed and eliminated and their number more than doubles by P21 when retinal circuits are mostly mature (P9: 753 ± 60 BC synapses/RGC, n = 6; P21: 1663 ± 180 BC synapses/RGC, n = 12; $p < 0.001$; mean ± SEM). By examining confocal image stacks of BC-RGC pairs plane-by-plane, we were able to count the number of synapses each BC axon made with the RGC dendrite (Figures 1C–1H). To be considered a synapse of the BC-RGC pair, PSD95-YFP puncta had to be localized in regions where the signal of BC axon and RGC dendrite overlapped. All BC-RGC pairs included in our analysis contained voxels of axo-dendritic overlap, but not all pairs were connected by synapses.

We found that between P9 and P21, B6 cells nearly doubled their connectivity with G10 RGCs (Figure 1I; P9: 2.7 ± 0.6 synapses/pair, n = 14; P21: 4.9 ± 0.6 synapses/pair, n = 35; $p < 0.01$). By contrast, B7 axons maintained a relatively constant number of synapses with G10 cells (P9: 3.1 ± 0.7 synapses/pair, n = 9; P21: 2.2 ± 0.7 synapses/pair, n = 13; $p > 0.2$), and RBs disconnected from G10 dendrites (P9: 1.4 ± 0.6 synapses/pair, n = 7; P21: 0 ± 0 synapses/pair, n = 14; $p < 0.001$). Thus, between P9 and P21—i.e., after laminar targeting is apparent—specific patterns of axonal connections emerge among converging BC inputs by differential formation, maintenance, and elimination of synapses with a shared RGC target.

Changes in Synaptic Conversion Underlie the Divergence of Axonal Connectivity

Several cellular mechanisms could account for the divergence of synaptic connectivity between the three BC types examined. The expectation based on observations of synaptic takeover at the NMJ might be that axons which increase their connectivity expand their territory and those that eliminate synapses shrink (Walsh and Lichtman, 2003). Because BC axons connect to several overlapping targets, however, they might not change their overall territory but rather realign with each target locally, such that axo-dendritic appositions become more frequent for BCs that gain synapses and contact sites are lost for those that eliminate synapses. Alternatively, the frequency with which axo-dendritic appositions bear synapses (i.e., connectivity fraction) could diverge as BC types adjust their connectivity.

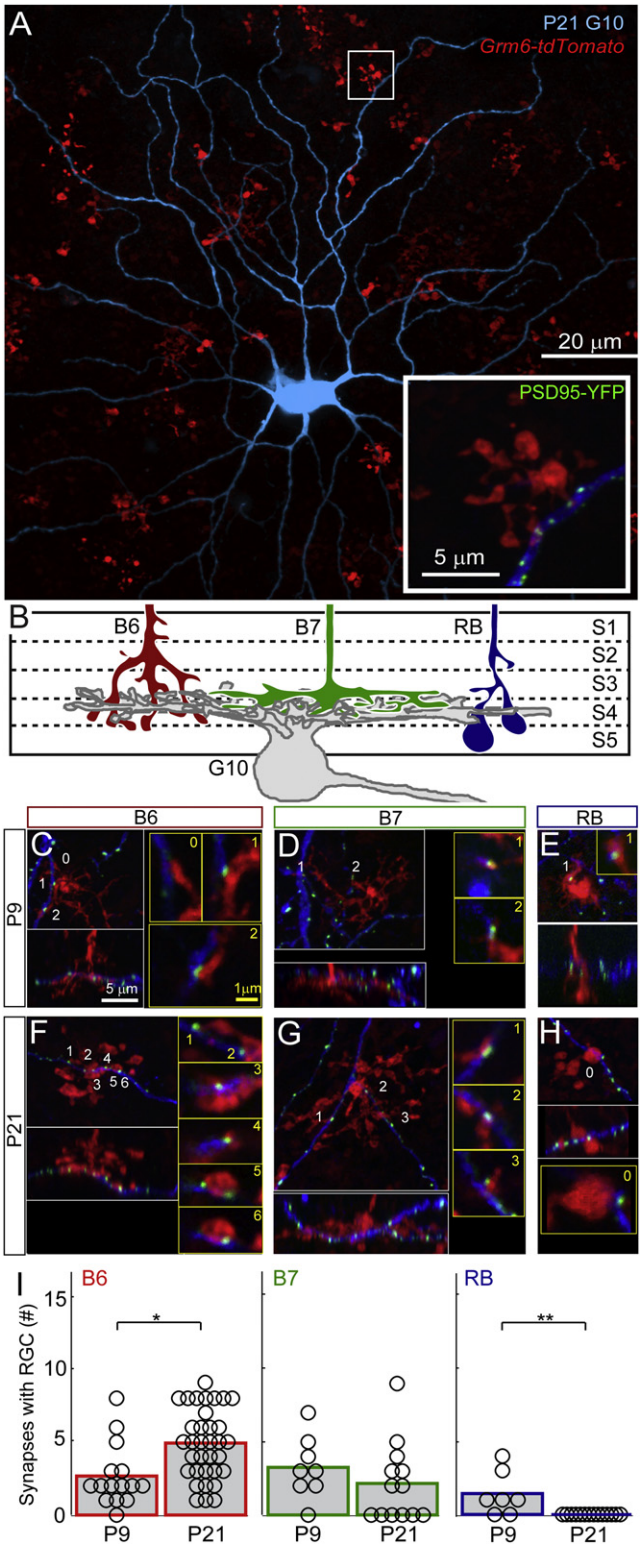

Figure 1. Divergent Synaptic Development of BC- RGC Pairs

(A) Overview image of a G10 RGC in a *Grm6-tdTomato* retina. Inset shows contact and synapses of a B6 axon with a G10 dendrite. (B) Schematic illustrating the laminar organization of B6, B7, and RB axons and G10 dendrites which overlap in sublamina 4 (S4) of the inner plexiform layer. (C–H) Examples of BC-G10 RGC pairs at P9 (C–E) and P21 (F–H) representing the development of synapses between B6 (C and F) B7 (D and G), and RB (E and H) axons and G10 dendrites. For each pair, the en face (top left panels) and orthogonal (bottom left panels) maximum intensity projections of confocal image stacks acquired on flat mount preparations are shown. Panels on the right display single planes from the confocal image stacks at contact points between BC axons and RGC dendrites in which axons (tdTomato), dendrites (CFP), and synapses (PSD95-YFP) are labeled. (I) Population data for the number of synapses between individual B6-G10 (left), B7-G10 (middle), and RB-G10 (right) pairs at P9 and P21. Each open circle represents one cell pair. Bars show the mean of the respective population; *$p < 0.05$, ** $p < 0.01$ (Wilcoxon-Mann-Whitney rank-sum test). See also Figure S1.

When we compared the axonal territories of each BC type at P9 and P21, we found that only the arbor size of B7 cells changed significantly (Figures 2A and 2B), the one cell type which maintained constant connectivity with G10 dendrites. To detect local adjustments in axonal and dendritic structure we counted appositions between each BC and RGC in a pair. These optically identified appositions (see Supplemental Information) are not guaranteed to represent contact between the membranes of two cells. However, they do require submicron proximity of processes and can therefore be used to measure the opportunities two cells have to form synapses (Stepanyants et al., 2002). While we observed some changes in the number of appositions between BCs and RGCs, these did not predict the changes in connectivity (Figures 2C and 2D). Instead, by comparing the number of synapses at each apposition (Figures 2E and 2F), it became clear that the divergence of input patterns from P9 to P21 is caused by selective changes in the frequency with which appositions from the different BC types are converted to synapses. At P9, all BC types examined contained synapses at about half their appositions with G10 dendrites ($p > 0.5$, ANOVA test). By P21, three distinct patterns emerged ($p < 0.001$, ANOVA test). B7 cells maintain a constant connectivity fraction (P9: 0.51 ± 0.11 synapses/apposition, $n = 9$; P21: 0.46 ± 0.15 synapses/apposition, $n = 13$; $p > 0.6$). RB cells, which keep appositions with G10 RGCs, lose all synapses from them (P9: 0.79 ± 0.41 synapses/apposition, $n = 7$; P21: 0 ± 0 synapses/apposition, $n = 14$; $p < 0.001$), and B6 cells increase the rate of conversion and typically form more than one synapse per apposition at P21 (P9: 0.60 ± 0.13 synapses/apposition, $n = 14$; P21: 1.35 ± 0.10 synapses/apposition, $n = 35$; $p < 0.001$).

Synapses Form and Are Eliminated in a Network of Relatively Stable Axo-Dendritic Appositions

Because synaptic rewiring from P9 to P21 appeared independent of changes in the number of appositions between BCs and RGCs (Figure 2), we wanted to test whether the formation and elimination of individual synapses was likewise uncoupled from the dynamics of axo-dendritic appositions. To address this question we generated transgenic mice in which nearly all ON BCs express YFP (*Grm6-YFP*; Figure S3) and biolistically labeled RGCs with tdTomato and PSD95-CFP. Time-lapse imaging every 2 hr for up to 18 hr revealed very little synaptic turnover at P21, supporting the notion that circuits are mostly mature at this age (data not shown). By contrast, at P9 we frequently observed synapse formation (1.3% ± 0.41% of synapses/hr, $n = 8$ cells)

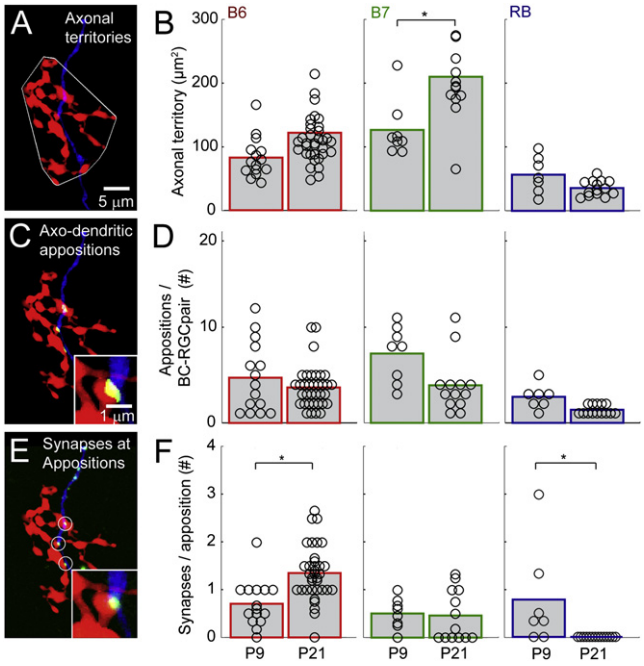

Figure 2. Selective Changes in Conversion of Contacts to Synapses Generate Specificity

(A) Axonal territories of BCs were measured as the area of the smallest convex polygon to encompass the arbor in a maximum intensity projection along the z axis of an image stack acquired from a flat mount preparation. (B) Population data showing the changes in territories occupied by B6 (left) B7, (middle), and RB (right) axons from P9 to P21. (C) Appositions between BC axons and RGC dendrites were defined as regions in the confocal image stack (x-y-z: 0.068-0.068-0.2 μm) where the two signals overlapped for >50 connected voxels. A high-magnification view of one apposition is shown in the inset. (D) The number of appositions between the different BC axons and G10 RGC dendrites is indicated for all cell pairs analyzed at P9 and P21. (E) The number of synapses at each apposition was counted combining automated detection of appositions with user identification of synapses based on plane-by-plane inspection of the image stacks. The inset shows a representative synapse of the cell pair at higher magnification. (F) Developmental changes in the connectivity fraction (i.e., the number of synapses per appositions) between B6 (left), B7 (middle), and RB (right) BCs and G10 RGCs are depicted. Throughout this figure, each circle represents average data from one cell pair, bars indicate the mean of the population and *$p < 0.05$ (Wilcoxon-Mann-Whitney rank-sum test). See also Figure S2.

and elimination events (0.77% ± 0.31% of synapses/hr) distributed throughout the RGC dendrite (Figures 3A–3C).

When we analyzed the presence of axo-dendritic appositions relative to the timing of synapse formation and elimination events at P9 (Figures 3D and 3E), it became evident that synaptic dynamics of BC-RGC pairs are not tightly linked to changes in appositions. Every one of 40 synapse formation events we observed during time-lapse imaging occurred at BC-RGC appositions that were present at the first time point of the series, 2–8 hr before synapse formation (Figures 3B and 3D). Similarly, most appositions persisted for many hours after synapse elimination (Figures 3C and 3E). While some appositions dissociated after synapse elimination, these events did not occur more frequently than expected by chance given the average stability of appositions without synapses (data not shown). Together, these results argue that converging excitatory inputs establish cell type-specific patterns of connections by differential synaptic conversion of relatively stable axo-dendritic appositions.

Neurotransmission Drives the Development of Multisynaptic Appositions and Shapes Synaptic Specificity

In our analysis of connectivity patterns we distinguished synaptic and nonsynaptic appositions based on the presence and absence, respectively, of PSD95-YFP puncta from sites of axo-dendritic overlap. In support of this distinction (Kerschensteiner et al., 2009; Morgan et al., 2008), we found that glutamate receptor subunits are enriched ~3-fold at appositions with PSD95-YFP clusters compared to those without (Figures S4A and S4B). In addition, ~98% of appositions with PSD95-YFP puncta also contained presynaptic release sites labeled with an antibody against the ribbon protein CtBP2, whereas ~92% of appositions lacking PSD95-YFP puncta did not (Figures S4C and S4D). At multisynaptic appositions formed by B6 cells each postsynaptic cluster was matched by a distinct presynaptic release site indicating that these contacts indeed contain multiple synapses (Figures 4A and 4B). Interestingly, the increase in B6-G10 connectivity from P9 to P21 is accounted for by a change in the frequency and distribution of multisynaptic appositions (Figure 4C).

To test the role of neurotransmission in the emergence of multisynaptic appositions and synaptic specificity, we crossed transgenic mice in which synaptic output from ON BCs is silenced by expression of the light chain of tetanus toxin (*Grm6-TeNT*) to *Grm6-tdTomato* mice (Kerschensteiner et al., 2009). In this background, we biolistically labeled G10 RGCs and their synapses with BCs. Analysis of the connectivity patterns of 89 cell pairs (Figure 4D) revealed that when glutamate release is blocked B6 BCs formed ~40% fewer synapses with G10 RGCs (WT: 4.9 ± 0.6 synapses/pair, n = 35; *Grm6-TeNT*: 2.9 ± 0.3 synapses/pair, n = 41; $p < 0.001$). By contrast, B7 BCs on average established the same number of connections with G10 RGCs (WT: 2.2 ± 0.7 synapses/pair, n = 13; *Grm6-TeNT*: 2.8 ± 0.6 synapses/pair, n = 13; $p > 0.3$) and synapses from RB cells were correctly eliminated from this target (WT: 0 ± 0 synapses/pair, n = 14; *Grm6-TeNT*: 0 ± 0 synapses/pair, n = 35). The selective reduction in B6-G10 connections is not explained by changes in the number of appositions between these cells (WT: 3.7 ± 0.4 appositions/pair; *Grm6-TeNT*: 4.0 ± 0.2 appositions/pair; $p > 0.2$). Instead, it was accounted for by an increase in appositions without synapses and a lack of multisynaptic appositions (Figure 4E). The distribution of synapses per apposition of B6-G10 pairs in *Grm6-TeNT* mice resembled those of wild-type mice at P9, arguing that in the absence of transmitter release their synaptic differentiation is arrested at an earlier stage of development.

DISCUSSION

To establish precisely wired neural circuits, developing axons need to select the correct synaptic partners among many available ones. In addition, functionally distinct axons often converge onto the same neuron and form specific patterns of connections with its dendrite (Shepherd, 2004). In recent years, cues that help

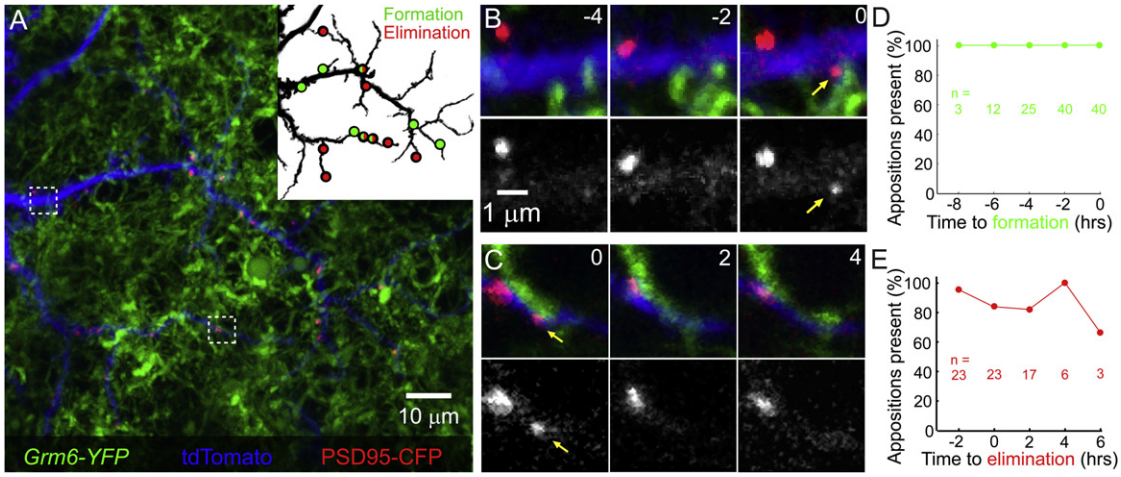

Figure 3. BC-RGC Synapses Form and Are Eliminated in a Network of Relatively Stable Appositions

(A) Dendrite of a G10 RGC biolistically labeled with tdTomato and PSD95-CFP in a transgenic mouse in which most ON bipolar cells express YFP (*Grm6-YFP*). For a characterization of this mouse line see Figure S3. Inset shows the distribution of synapse formation (green circles) and elimination (red circles) events observed during 12 hr of live imaging. (B and C) Time series of the regions indicated in (A) in which a PSD95 cluster forms (B) and another is eliminated (C) at pre-existing and persisting axo-dendritic appositions, respectively. Merged images are shown in the top rows, the isolated PSD95-CFP signal below. Arrows point to the synapse formation (B) and elimination (C) events. (D–E) Plot illustrating how long axo-dendritic appositions preceded the formation of synapses (D) and persisted after synapse elimination (E) (n = number of observations). See also Figure S3.

axons adhere to correct and avoid incorrect targets have been identified (Sanes and Yamagata, 2009; Waites et al., 2005). By contrast, no study has yet examined the development of synapses from functionally distinct axons with a shared target dendrite. By reconstructing the axons and synaptic connections of three retinal BC types contacting the dendrites of a single type of RGC, we identified developmental mechanisms that confer specificity to the synaptic patterns of converging inputs and discovered novel synaptic arrangements in the retina.

As in many other neural circuits, connections between BCs and RGCs in the retina are organized into functionally and anatomically distinct layers (Masland, 2001; Sanes and Yamagata, 1999; Sanes and Zipursky, 2010; Wässle, 2004). Within each layer, RGCs can receive input from more than one type of BC (Freed and Sterling, 1988; McGuire et al., 1984). Together, converging BC types, which communicate different aspects of the photoreceptor signal, shape the temporal, spatial, and spectral properties of RGC light responses (Breuninger et al., 2011; Freed, 2000; Li and DeVries, 2006). Here, we found that B6 and B7 BCs connect through distinct synaptic arrangements with G10 RGCs. In the mature retina, B7 axonal boutons contact single glutamatergic postsynaptic sites, whereas individual B6 boutons are frequently associated with multiple postsynaptic densities on the G10 dendrite each matched by a separate release site. A BC synapse with multiple ribbons had previously been observed at the ultrastructural level on a direction-selective RGC in the rabbit retina (Famiglietti, 2005), but the identity of the BC was unknown. Also, whether each ribbon was apposed to its own postsynaptic site was not resolved. The multisynaptic appositions we report here thus represent a novel synaptic constellation in retinal circuits. While the functional properties of multisynaptic appositions remain to be determined, we predict that synaptic drive from B6 BCs to G10 RGCs is robust, perhaps in ways analogous to signal transmission at the Calyx of Held (Schneggenburger and Forsythe, 2006). In addition, the clustering of synaptic connections may predispose B6 BCs to trigger dendritic spikes in G10 RGCs (Larkum and Nevian, 2008).

The laminar organization of the retina allowed us to determine when synaptic specificity emerges relative to the timing of axonal and dendritic targeting. We found that as developing BC axons become restricted to their target layer, G10 dendrites connect similarly to B6, B7, and RB BCs. Subsequently, the synaptic patterns of these three inputs diverge. While this had not been studied at the level of cell type specificity before, the general sequence of lamination before synaptic specificity is reminiscent of observations made on thalamocortical projections to primary visual cortex (V1) in cat, ferret, and primate (Katz and Shatz, 1996). In V1, axons from the dorsolateral geniculate nucleus of the thalamus appropriately target cortical layer 4 before rearranging synapses to produce ocular dominance columns. More studies are needed to determine how general a theme the developmental separation of axo-dendritic targeting and synaptic refinement is in laminar circuit assembly.

Our reconstructions and live imaging of BC-RGC synaptogenesis provide insight into the cellular mechanisms by which input-specific patterns of connections with a shared postsynaptic neuron can arise. Synaptic development of axons in vivo had previously been studied at the NMJ and for climbing fiber inputs to Purkinje cells. In both cases, convergence is transient and axons that lose their connections are retracted, whereas those that increase connectivity expand. By contrast, RB terminals remain closely apposed to G10 dendrites even as their synapses are eliminated and B6 axons do not grow in spite of increasing their connectivity. These findings suggest that synaptic connectivity is determined by factors other than axo-dendritic overlap (Ohki and Reid, 2007; Stepanyants and Chklovskii,

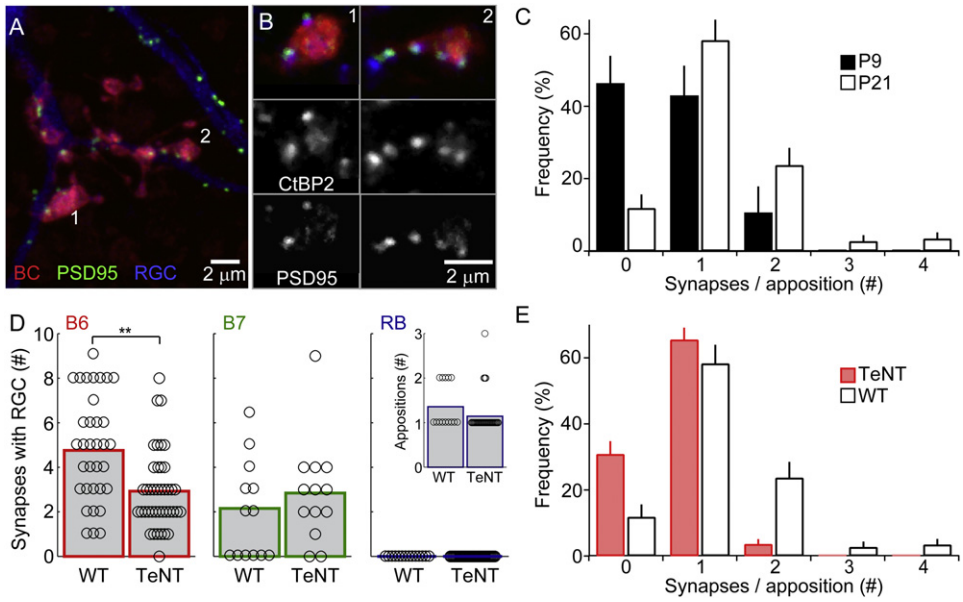

Figure 4. Neurotransmission Regulates Synaptic Differentiation in a Cell Type-Dependent Manner

(A and B) Example of a B6-G10 pair for which both postsynaptic densities (PSD95-YFP) and presynaptic release sites (anti-CtBP2) were labeled. The CtBP2 signal was multiplied by a binary mask of the B6 BC based on its tdTomato expression to identify release sites of the presynaptic cell in the pair. Each postsynaptic density at multisynaptic appositions is matched by a different release site. (C) Histograms of the distribution of different synaptic arrangements at P9 and P21 show that the increase in B6-G10 connectivity is caused by a shift toward multisynaptic appositions including those of higher order. (D) Summary data comparing the number of synapses between B6 - G10 (left), B7-G10 (middle), and RB-G10 (right) pairs in wild-type (WT) and *Grm6-TeNT* (TeNT) mice at P21. For ease of comparison, wild-type data identical to Figure 1H are reproduced here. Each open circle represents one cell pair. Bars show the mean of the respective population; $^{**}p < 0.01$ (Wilcoxon-Mann-Whitney rank-sum test). The number of appositions between RB and G10 RGCs is shown in the inset of the right panel. (E) Histograms comparing the distribution of synapses per appositions in wild-type (same data set as in C) and *Grm6-TeNT* mice suggest that glutamate release from BCs drives synaptic differentiation of B6-G10 contacts, in particular the formation of multisynaptic appositions. Bars (error bars) in (C) and (E) indicate mean (±SEM) of the respective data sets. See also Figure S4.

2005). In the field of neurogeometry, close appositions of axons and dendrites are referred to as potential synapses (Stepanyants et al., 2002). In Peter's rule, it was proposed that knowing potential connectivity may be sufficient to predict the wiring of neural circuits (Peters and Feldman, 1976; Stepanyants et al., 2002). Recent studies have identified several deviations from Peter's rule (Kalisman et al., 2005; Mishchenko et al., 2010; Shepherd et al., 2005; Song et al., 2005). Whether the conversion from potential to actual synapses changes during development remained unknown. By labeling not only axons and dendrites of identified pairs of neurons, but also the synapses between them, we discovered that B6, B7, and RB BCs uniformly convert about half their appositions with G10 RGC dendrites into synapses as their axons complete laminar targeting. During the ensuing period of refinement, however, the patterns of BC connectivity diverge by cell type-specific changes in the conversion of potential to actual synapses. This suggests that initial synaptogenesis is relatively unspecific and connectivity of early neural networks may accurately be predicted by neuronal geometry. With maturation, however, Peter's rule breaks down as synaptic specificity is generated by cell type-specific changes in the connectivity fraction. In the retina, and possibly other laminar circuits, axonal and dendritic stratification thus restrict potential connectivity, and the differential conversion of potential to actual synapses then sculpts cell type-specific patterns of connectivity among axons and dendrites that colaminate.

It is interesting to consider the appearance and disappearance of BC-RGC synapses in a network of relatively stable axo-dendritic appositions which we observe in situ in the context of studies on synaptogenesis among cultured hippocampal neurons. Excitatory synapses on pyramidal neurons in this system often form within 1–2 hr after dendritic filopodia first contact nearby axons (Bresler et al., 2001; Friedman et al., 2000; Okabe et al., 2001). While some studies noted that many new contacts did not mature into synapses during the ~2 hr period of observation, it remained unclear whether they were later converted (Bresler et al., 2001; Friedman et al., 2000). For all synapse formation events we observed between BCs and RGCs, appositions were present at the first frame of the imaging series, up to 8 hr before the recruitment of PSD95. Similar observations were recently made for the formation of GABAergic connections in hippocampal slice cultures (Wierenga et al., 2008). One interpretation, since both GABAergic connections onto pyramidal neurons and glutamatergic synapses onto RGCs form on dendritic shafts, is that the inductive role of axo-dendritic contact is a specific adjustment to the formation of spine synapses (Yuste and Bonhoeffer, 2004). In hippocampal circuits, excitatory axons run perpendicular to dendrites such that contact opportunities are limited and filopodia might be necessary to sample passing axons (Chklovskii et al., 2004). By contrast, in the retina BC axons and RGC dendrites branch in parallel such that contact opportunities are abundant and

connectivity can change without axo-dendritic rearrangements. Thus, the layout of axons and dendrites (e.g., parallel versus perpendicular) in a circuit may inform the rules and mechanisms that guide its synaptic development.

Throughout the nervous system the development of synaptic specificity appears to require the collaboration of several mechanisms. Adhesive and repulsive interactions between correct and incorrect synaptic partners, respectively, have been shown to guide cell-target recognition (Matsuoka et al., 2011; Sanes and Yamagata, 2009). In addition, both membrane-bound and diffusible signals that can selectively promote the formation of inhibitory or excitatory synapses have been identified (Chih et al., 2005; Linhoff et al., 2009; Terauchi et al., 2010). Here, we discovered that neurotransmission differentially regulates synaptogenesis of converging excitatory BC inputs with a shared RGC target. B6 BCs fail to form characteristic multisynaptic appositions with G10 RGCs when they are unable to release glutamate. By contrast, the average number of synapses between B7 BCs and G10 RGCs was unchanged in *mGluR6-TeNT* mice and RB synapses are correctly eliminated from this target. Because we have previously shown that the overall number of output synapses for all three of these BC types is similarly reduced (Kerschensteiner et al., 2009), our current results suggest that the influence of neurotransmission on synaptogenesis depends on the combination of pre- and postsynaptic cell type. In this way, synaptic activity differentially regulates the connectivity patterns of converging excitatory inputs, and provides an interesting addition to the signals that regulate synaptic specificity in developing circuits.

EXPERIMENTAL PROCEDURES

Transgenic Mice

To visualize isolated B6, B7, and RB BCs, we generated transgenic mice in which a ~9 kb fragment of the *Grm6* promoter drove expression of the red fluorescent protein tandem dimer Tomato (tdTomato) and selected a founder line in which position effect variegation limited strong labeling to few dispersed ON bipolar cells (*Grm6-tdTomato*). In addition, we generated transgenic mice in which the same promoter fragment drove expression of yellow fluorescent protein (YFP) in most ON bipolar cells (*Grm6-YFP*).

Tissue Preparation

Animal protocols were approved by the Washington University School of Medicine Animal Studies Committee and the Institutional Animal Care and Use Committee at the University of Washington. All procedures were in compliance with the National Institutes of Health Guide for the Care and Use of Laboratory Animals. Mice deeply anaesthetized with isoflurane or CO_2 were decapitated and enucleated. Each cornea was punctured with a 30 gauge needle and the eyes placed in cold oxygenated mouse artificial cerebrospinal fluid (mACSF) containing (in mM): 119 NaCl, 2.5 KCl, 2.5 $CaCl_2$, 1.3 $MgCl_2$, 1 NaH_2PO_4, 11 glucose, and 20 HEPES. The pH of mACSF was adjusted to 7.37 with NaOH. For vibratome sections, the lens and vitreous were removed and the remaining eye cup fixed for 30 min in 4% paraformaldehyde in mACSF. For flat-mount preparations, the retina was isolated and mounted retinal ganglion cell (RGC) side up on membrane discs (Millipore).

Biolistic Transfection

Gold particles (12.5 mg, 1.6 μm diameter, Bio-Rad), were coated with plasmids using the cytomegalovirus promoter to express a cytosolic fluorescent protein—tdTomato or cerulean fluorescent protein (CFP)—and postsynaptic density protein 95 (PSD95) fused at its C terminus to CFP or YFP (Morgan and Kerschensteiner, 2011). Twenty micrograms of the plasmid encoding the cytosolic label were combined with 10 μg of the PSD95 plasmid. We used a Helios Gene gun (~40 psi, Bio-Rad) to deliver gold particles to RGCs and transferred flat-mount preparations to a humid oxygenated chamber heated to 33°C for 14–18 hr. The tissue was then either transferred to a live imaging chamber or fixed for 30 min in 4% paraformaldehyde in mACSF (Williams et al., 2010).

Immunohistochemistry

Fixed retinal flat mounts were incubated with primary antibodies against PKCα (1:1000, Sigma), synaptotagmin 2 (Znp-1, 1:1000, Zebrafish International Resource Center), CtBP2 (1:1000, BD Bioscience), or GluR2/3 (1:1000, Upstate) for 3–7 days at 4°C, washed and incubated with secondary antibodies (Alexa 488, 568, or 633 conjugates, 1:1000, Invitrogen) overnight at 4°C.

Imaging

Image stacks were acquired on Olympus FV1000 or FV300 laser scanning confocal microscopes. Fixed tissue was imaged using a 1.35NA 60× oil immersion objective at a voxel size of 0.068-0.068-0.2 μm (x-y-z). For live imaging we used a 1.1NA 60× water immersion objective and identical voxel size. To monitor synaptogenesis, retinal flat mount preparations were continuously perfused with oxygenated mACSF (1–2 ml / min) heated to 33°C and imaged every 2 hr for up to 18 hr. Images were analyzed using Amira (Visage Imaging) and custom software written in Matlab (see Supplemental Experimental Procedures).

SUPPLEMENTAL INFORMATION

Supplemental Information includes four figures and Supplemental Experimental Procedures and can be found with this article online at doi:10.1016/j.neuron.2011.08.025.

ACKNOWLEDGMENTS

We thank members of the Wong and Kerschensteiner laboratories for comments on the manuscript. This work was supported by an NEI Training grant EY 07031 (University of Washington, J.L.M.), NIH grants EY10699, EY17101, and J.S. McDonnell Foundation (R.O.L.W.), the Alfred P. Sloan Foundation, the Whitehall Foundation, the Hope for Vision Foundation, and the Edward Mallinckrodt Jr. Foundation (D.K.).

Accepted: August 12, 2011
Published: September 21, 2011

REFERENCES

Bresler, T., Ramati, Y., Zamorano, P.L., Zhai, R., Garner, C.C., and Ziv, N.E. (2001). The dynamics of SAP90/PSD-95 recruitment to new synaptic junctions. Mol. Cell. Neurosci. *18*, 149–167.

Breuninger, T., Puller, C., Haverkamp, S., and Euler, T. (2011). Chromatic bipolar cell pathways in the mouse retina. J. Neurosci. *31*, 6504–6517.

Brown, M.C., Jansen, J.K., and Van Essen, D. (1976). Polyneuronal innervation of skeletal muscle in new-born rats and its elimination during maturation. J. Physiol. *261*, 387–422.

Chih, B., Engelman, H., and Scheiffele, P. (2005). Control of excitatory and inhibitory synapse formation by neuroligins. Science *307*, 1324–1328.

Chklovskii, D.B., Mel, B.W., and Svoboda, K. (2004). Cortical rewiring and information storage. Nature *431*, 782–788.

Coombs, J.L., Van Der List, D., and Chalupa, L.M. (2007). Morphological properties of mouse retinal ganglion cells during postnatal development. J. Comp. Neurol. *503*, 803–814.

Diao, L., Sun, W., Deng, Q., and He, S. (2004). Development of the mouse retina: emerging morphological diversity of the ganglion cells. J. Neurobiol. *61*, 236–249.

Famiglietti, E.V. (2005). Synaptic organization of complex ganglion cells in rabbit retina: type and arrangement of inputs to directionally selective and local-edge-detector cells. J. Comp. Neurol. *484*, 357–391.

Fox, M.A., and Sanes, J.R. (2007). Synaptotagmin I and II are present in distinct subsets of central synapses. J. Comp. Neurol. *503*, 280–296.

Freed, M.A. (2000). Parallel cone bipolar pathways to a ganglion cell use different rates and amplitudes of quantal excitation. J. Neurosci. *20*, 3956–3963.

Freed, M.A., and Sterling, P. (1988). The ON-alpha ganglion cell of the cat retina and its presynaptic cell types. J. Neurosci. *8*, 2303–2320.

Friedman, H.V., Bresler, T., Garner, C.C., and Ziv, N.E. (2000). Assembly of new individual excitatory synapses: time course and temporal order of synaptic molecule recruitment. Neuron *27*, 57–69.

Ghosh, K.K., Bujan, S., Haverkamp, S., Feigenspan, A., and Wässle, H. (2004). Types of bipolar cells in the mouse retina. J. Comp. Neurol. *469*, 70–82.

Hashimoto, K., Ichikawa, R., Kitamura, K., Watanabe, M., and Kano, M. (2009). Translocation of a "winner" climbing fiber to the Purkinje cell dendrite and subsequent elimination of "losers" from the soma in developing cerebellum. Neuron *63*, 106–118.

Haverkamp, S., Grünert, U., and Wässle, H. (2001a). Localization of kainate receptors at the cone pedicles of the primate retina. J. Comp. Neurol. *436*, 471–486.

Haverkamp, S., Grünert, U., and Wässle, H. (2001b). The synaptic architecture of AMPA receptors at the cone pedicle of the primate retina. J. Neurosci. *21*, 2488–2500.

Kalisman, N., Silberberg, G., and Markram, H. (2005). The neocortical microcircuit as a tabula rasa. Proc. Natl. Acad. Sci. USA *102*, 880–885.

Katz, L.C., and Shatz, C.J. (1996). Synaptic activity and the construction of cortical circuits. Science *274*, 1133–1138.

Kerschensteiner, D., Morgan, J.L., Parker, E.D., Lewis, R.M., and Wong, R.O. (2009). Neurotransmission selectively regulates synapse formation in parallel circuits in vivo. Nature *460*, 1016–1020.

Larkum, M.E., and Nevian, T. (2008). Synaptic clustering by dendritic signalling mechanisms. Curr. Opin. Neurobiol. *18*, 321–331.

Li, W., and DeVries, S.H. (2006). Bipolar cell pathways for color and luminance vision in a dichromatic mammalian retina. Nat. Neurosci. *9*, 669–675.

Linhoff, M.W., Laurén, J., Cassidy, R.M., Dobie, F.A., Takahashi, H., Nygaard, H.B., Airaksinen, M.S., Strittmatter, S.M., and Craig, A.M. (2009). An unbiased expression screen for synaptogenic proteins identifies the LRRTM protein family as synaptic organizers. Neuron *61*, 734–749.

Masland, R.H. (2001). The fundamental plan of the retina. Nat. Neurosci. *4*, 877–886.

Masu, M., Iwakabe, H., Tagawa, Y., Miyoshi, T., Yamashita, M., Fukuda, Y., Sasaki, H., Hiroi, K., Nakamura, Y., Shigemoto, R., et al. (1995). Specific deficit of the ON response in visual transmission by targeted disruption of the mGluR6 gene. Cell *80*, 757–765.

Matsuoka, R.L., Nguyen-Ba-Charvet, K.T., Parray, A., Badea, T.C., Chédotal, A., and Kolodkin, A.L. (2011). Transmembrane semaphorin signalling controls laminar stratification in the mammalian retina. Nature *470*, 259–263.

McGuire, B.A., Stevens, J.K., and Sterling, P. (1984). Microcircuitry of bipolar cells in cat retina. J. Neurosci. *4*, 2920–2938.

Mishchenko, Y., Hu, T., Spacek, J., Mendenhall, J., Harris, K.M., and Chklovskii, D.B. (2010). Ultrastructural analysis of hippocampal neuropil from the connectomics perspective. Neuron *67*, 1009–1020.

Morgan, J.L., and Kerschensteiner, D. (2011). Ballistic Labelling of Developing Retinal Neurons. In Imaging in Developmental Biology, J. Sharpe and R.O. Wong, eds. (Cold Spring Harbor, NY: Cold Spring Harbor Laboratory Press), pp. 177–190.

Morgan, J.L., Dhingra, A., Vardi, N., and Wong, R.O. (2006). Axons and dendrites originate from neuroepithelial-like processes of retinal bipolar cells. Nat. Neurosci. *9*, 85–92.

Morgan, J.L., Schubert, T., and Wong, R.O. (2008). Developmental patterning of glutamatergic synapses onto retinal ganglion cells. Neural Develop. *3*, 8.

Nomura, A., Shigemoto, R., Nakamura, Y., Okamoto, N., Mizuno, N., and Nakanishi, S. (1994). Developmentally regulated postsynaptic localization of a metabotropic glutamate receptor in rat rod bipolar cells. Cell *77*, 361–369.

Ohki, K., and Reid, R.C. (2007). Specificity and randomness in the visual cortex. Curr. Opin. Neurobiol. *17*, 401–407.

Okabe, S., Miwa, A., and Okado, H. (2001). Spine formation and correlated assembly of presynaptic and postsynaptic molecules. J. Neurosci. *21*, 6105–6114.

Peters, A., and Feldman, M.L. (1976). The projection of the lateral geniculate nucleus to area 17 of the rat cerebral cortex. I. General description. J. Neurocytol. *5*, 63–84.

Sanes, J.R., and Yamagata, M. (1999). Formation of lamina-specific synaptic connections. Curr. Opin. Neurobiol. *9*, 79–87.

Sanes, J.R., and Yamagata, M. (2009). Many paths to synaptic specificity. Annu. Rev. Cell Dev. Biol. *25*, 161–195.

Sanes, J.R., and Zipursky, S.L. (2010). Design principles of insect and vertebrate visual systems. Neuron *66*, 15–36.

Schneggenburger, R., and Forsythe, I.D. (2006). The calyx of Held. Cell Tissue Res. *326*, 311–337.

Shepherd, G.M., ed. (2004). The Synaptic Organization of the Brain, Fifth Edition (Oxford: Oxford University Press, Inc.).

Shepherd, G.M., Stepanyants, A., Bureau, I., Chklovskii, D., and Svoboda, K. (2005). Geometric and functional organization of cortical circuits. Nat. Neurosci. *8*, 782–790.

Silver, R.A. (2010). Neuronal arithmetic. Nat. Rev. Neurosci. *11*, 474–489.

Song, S., Sjöström, P.J., Reigl, M., Nelson, S., and Chklovskii, D.B. (2005). Highly nonrandom features of synaptic connectivity in local cortical circuits. PLoS Biol. *3*, e68. 10.1371/journal.pbio.0030068.

Spruston, N. (2008). Pyramidal neurons: dendritic structure and synaptic integration. Nat. Rev. Neurosci. *9*, 206–221.

Stacy, R.C., and Wong, R.O. (2003). Developmental relationship between cholinergic amacrine cell processes and ganglion cell dendrites of the mouse retina. J. Comp. Neurol. *456*, 154–166.

Stepanyants, A., and Chklovskii, D.B. (2005). Neurogeometry and potential synaptic connectivity. Trends Neurosci. *28*, 387–394.

Stepanyants, A., Hof, P.R., and Chklovskii, D.B. (2002). Geometry and structural plasticity of synaptic connectivity. Neuron *34*, 275–288.

Terauchi, A., Johnson-Venkatesh, E.M., Toth, A.B., Javed, D., Sutton, M.A., and Umemori, H. (2010). Distinct FGFs promote differentiation of excitatory and inhibitory synapses. Nature *465*, 783–787.

Vardi, N., Duvoisin, R., Wu, G., and Sterling, P. (2000). Localization of mGluR6 to dendrites of ON bipolar cells in primate retina. J. Comp. Neurol. *423*, 402–412.

Völgyi, B., Chheda, S., and Bloomfield, S.A. (2009). Tracer coupling patterns of the ganglion cell subtypes in the mouse retina. J. Comp. Neurol. *512*, 664–687.

Waites, C.L., Craig, A.M., and Garner, C.C. (2005). Mechanisms of vertebrate synaptogenesis. Annu. Rev. Neurosci. *28*, 251–274.

Walsh, M.K., and Lichtman, J.W. (2003). In vivo time-lapse imaging of synaptic takeover associated with naturally occurring synapse elimination. Neuron *37*, 67–73.

Wässle, H. (2004). Parallel processing in the mammalian retina. Nat. Rev. Neurosci. *5*, 747–757.

Wässle, H., Puller, C., Müller, F., and Haverkamp, S. (2009). Cone contacts, mosaics, and territories of bipolar cells in the mouse retina. J. Neurosci. *29*, 106–117.

Wierenga, C.J., Becker, N., and Bonhoeffer, T. (2008). GABAergic synapses are formed without the involvement of dendritic protrusions. Nat. Neurosci. *11*, 1044–1052.

Williams, M.E., de Wit, J., and Ghosh, A. (2010). Molecular mechanisms of synaptic specificity in developing neural circuits. Neuron *68*, 9–18.

Yuste, R., and Bonhoeffer, T. (2004). Genesis of dendritic spines: insights from ultrastructural and imaging studies. Nat. Rev. Neurosci. *5*, 24–34.